



Article

Characterization of Inclusion Size Distributions in Steel Wire Rods

Pablo Huazano-Estrada ¹, Martín Herrera-Trejo ^{1,*}, Manuel de J. Castro-Román ¹  and Jorge Ruiz-Mondragón ² 

¹ Centro de Investigación y de Estudios Avanzados, CINVESTAV Saltillo, Av. Industria Metalúrgica No. 1062, Parque Industrial Saltillo-Ramos Arizpe, Ramos Arizpe 25900, Mexico

² COMIMSA, Saltillo 25290, Mexico

* Correspondence: martin.herrera@cinvestav.edu.mx; Tel.: +52-844-438-9643

Abstract: The control of inclusions in steel components is essential to guarantee strong performance. The reliable characterization of inclusion populations is essential not only to evaluate the quality of the components but also to allow the use of analytical procedures for the comparison and discrimination of inclusion populations. In this work, inclusion size distributions in wire rod specimens from six plant-scale heats were measured and analyzed. For the measurements, the metallographic procedure specified in the ASTM E2283 standard was used. The population density function (PDF) approach and the extreme value statistical procedure specified in the ASTM E2283 standard were used to analyze the whole size distribution and the upper tail of the size distribution, respectively. The PDF approach allowed us to identify differences among inclusion size distributions and showed that new inclusions were not formed after the liquid steel treatment process. The extreme value statistical procedure led to the prediction of the maximum inclusion length for each heat, which was used for the statistical discrimination of heats. Furthermore, the estimation of the probability of finding an inclusion larger than a given inclusion size using the extreme value theory allowed us to order the heats for different critical inclusion sizes.

Keywords: inclusion; size distribution; population density function; extreme value theory



Citation: Huazano-Estrada, P.; Herrera-Trejo, M.; Castro-Román, M.d.J.; Ruiz-Mondragón, J. Characterization of Inclusion Size Distributions in Steel Wire Rods. *Materials* **2022**, *15*, 7681. <https://doi.org/10.3390/ma15217681>

Academic Editors: Konstantin Borodianskiy and Andrea Di Schino

Received: 16 September 2022

Accepted: 18 October 2022

Published: 1 November 2022

Publisher's Note: MDPI stays neutral with regard to jurisdictional claims in published maps and institutional affiliations.



Copyright: © 2022 by the authors. Licensee MDPI, Basel, Switzerland. This article is an open access article distributed under the terms and conditions of the Creative Commons Attribution (CC BY) license (<https://creativecommons.org/licenses/by/4.0/>).

1. Introduction

Control over inclusion cleanliness in steel products is necessary to ensure their performance under specific conditions. Inclusion size distribution is one of the parameters used to evaluate steel quality, and therefore its control during the steelmaking process is required [1,2]. Hence, the successful control of the inclusion size distribution must be based on analysis procedures that provide information on the formation and evolution of inclusions. Furthermore, predictive and discriminative analysis procedures are desirable.

The size distribution of an inclusion population is frequently estimated from metallography measurements and image analysis and represents an inclusion cleanliness parameter. Higgings [3] represented the particle size distribution by the population density function (PDF) as an alternative to the classic histogram format. The PDF approach presents the advantage of being user-independent compared to the histogram and the corresponding density function, which assumes a normal distribution [4]. Furthermore, the PDF is unique for a given inclusion population, provides information on the formation and evolution of inclusions [5] and enables the comparison of size distributions from different specimens. The logarithmic representation of PDFs is linear or quadratic and can be described by fractal (power law) and lognormal distributions, respectively [6]. Zinngrebe et al. [7] introduced the PDF approach in the analysis of inclusion size distribution and used it to study the formation of inclusions during the secondary steelmaking and casting process of Ti-alloyed Al-killed steel. The logarithmic representation of PDF showed a quadratic shape just after Al addition and became linear with time. A quadratic shape characterizes the transient de-oxidation process where the transfer of the matter occurs between steel and inclusions, i.e.,

the formation and growth of inclusion process, whereas a linear behavior indicates that the equilibrium inclusion-steel was reached, and consequently the inclusion size distribution is the result of effective collisions and breakage phenomena and the removal of inclusions. Hence, it is expected that estimated PDFs in specimens obtained in later stages of processing can provide information on the size distribution at the end of the liquid steel treatment and its subsequent evolution. This provides evidence of the occurrence of phenomena, such as the reoxidation process, that form new inclusions after liquid treatment. It is worth mentioning recent works that use the PDF approach. Piva and Pistorius [8] used the PDF to show the evolution of the size distribution for different processing routes for steel Ca treatment, while Qifeng et al. [9] used it to analyze results obtained from the modeling of the nucleation, growth, and agglomeration of Al_2O_3 inclusions.

On the other hand, the generalized extreme value (GEV) theory based on Murakami et al.'s pioneering work [10] has been used to describe the large inclusion size tail of the size distribution, in which standard probability distributions, such as the log-normal distribution, are insufficient [4]. The method is based on measuring the maximum inclusion size in random inspection areas and fitting the Gumbel distribution to these measurements. This allows to predict the maximum inclusion length (L_{max}), i.e., the longest inclusion expected to be found in a predetermined area. The fitting of the Gumbel distribution to the size distributions of different specimens enables the statistical comparison and discrimination of L_{max} . Variations in the procedures used for the application of GEV led to the development of the ASTM E2283 standard "Standard Practice for Extreme Value Analysis of Nonmetallic Inclusions in Steel and other Microstructural Features" [11] as a guide to evaluate inclusion cleanliness. The standard was shown to be a reliable tool to assess inclusion cleanliness. Recently, Kumar and Balachandran [12] showed the standard as an effective tool for estimating the largest inclusion, which has the potential for crack nucleation that leads to fatigue failure in steel specimens. Fuchs et al. [13] confirmed the effectiveness of the standard in the evaluation of inclusion cleanliness in ultraclean gear steels. Furthermore, the standard has been used in the evaluation of the maximum inclusion size of heat-treated wire rod specimens [14]. More recently, the results using the standard showed relatively good agreement with measurements of large inclusions based on the X-ray microcomputed tomography method [15]

In this work, size distributions were measured in steel wire rod specimens from six different plant-scale heats following the metallographic procedure indicated in the ASTM E2283 standard. The PDF approach was used to analyze the whole size distribution, whereas the GEV theory was employed to describe the upper tail of the size distributions following the procedure specified in the ASTM E2283 standard and to estimate the survival probability.

2. Background

2.1. PDF Approach

The PDF concept, introduced by Higgins [3], is expressed by the following equation:

$$PDF = \frac{n_v(L_{XY})}{(L_Y - L_X)} \quad (1)$$

where $n_v(L_{XY})$ is the frequency of inclusions in a given size bin (particle number per volume), and $(L_Y - L_X)$ is the bin width with units of length. The logarithmic representation of PDFs can be linear or quadratic and can be described by fractal (power law) and lognormal distributions, respectively [6]. The probability density function of the fractal distribution is given by

$$f(x) = \frac{C}{x^D} \quad (2)$$

where C is the constant of proportionality, and D is the fractal dimension. The probability density function of the lognormal distribution is

$$f(x) = \frac{1}{x \sigma (2\pi)^{1/2}} \exp \left[-\frac{[\ln(x) - \ln(\mu)]^2}{2\sigma^2} \right] \quad (3)$$

where m and s are the mean and standard deviation, respectively.

2.2. ASTM E2283 Standard

The ASTM E2283 standard [11] describes a procedure to statistically characterize the distribution of the largest particles in a solid matrix. It can be used in the case of inclusions in a steel matrix. Herein, essential aspects allowing us to understand the use of the standard in this work are introduced.

The ASTM E2283 procedure is based upon quantitative optical metallographic measurements and their analysis via statistical GEV theory. Six specimens per analysis are required for metallographic measurements. An area of 150 mm² (control area A_0) must be evaluated in four different metallographically prepared planes in each specimen, and the largest measured inclusion in each A_0 is recorded. The measurements must be made using the correct magnification to ensure that the detected largest inclusion is a minimum of 20 pixels in length. The procedure provides a dataset of the 24 largest inclusions, which are listed in ascending order and can be represented as x_i . The cumulative probability P_i is calculated by the following equation:

$$P_i = \frac{x_i}{(N + 1)} \quad (4)$$

where $N = 24$.

The prediction of L_{max} is based on the fitting of the Gumbel extreme value distribution to the 24 recorded inclusion lengths. The probability density function of the Gumbel distribution is expressed by

$$f(x) = \frac{1}{\delta} \left[\exp \left(-\frac{x - \lambda}{\delta} \right) \right] \times \exp \left[-\exp \left(-\frac{x - \lambda}{\delta} \right) \right] \quad (5)$$

where x is the random variable (maximum inclusion length), and l and d are the location and scale parameters, respectively. The corresponding cumulative distribution is

$$F(x) = \exp \left(-\exp \left(-\frac{x - \lambda}{\delta} \right) \right) \quad (6)$$

which can be rewritten by introducing the reduced variate y :

$$F(y) = \exp(-\exp(-y)) \quad (7)$$

where

$$y = \frac{x - \lambda}{\delta} \quad (8)$$

Solving Equation (8) for x ,

$$x = \delta y + \lambda \quad (9)$$

From Equation (7), y can be expressed in terms of the cumulative function as

$$y = -\ln(-\ln(F(y))) \quad (10)$$

Equation (10) can be related to Equation (4), and the expression for y is rewritten as

$$y = -\ln(-\ln(F(y))) = -\ln(-\ln(P)) \quad (11)$$

On the other hand, the return period T is used to predict how large an inclusion could be expected to be found if a reference area (A_{ref}) larger than A_o were to be evaluated. That is,

$$T = \frac{A_{ref}}{A_o} \quad (12)$$

In the ASTM E2283 standard, A_{ref} is chosen to be 1000 times larger than A_o . Furthermore, T is statistically defined as

$$T = \frac{1}{1 - P} \quad (13)$$

For a T value of 1000, the corresponding P value is 0.999 (99.9%).

Thus, for $P = 0.999$, the $y_{(P=0.99)}$ value is calculated using Equation (11), and the corresponding $x_{(P=0.99)}$ value is calculated by Equation (9). The calculated $x_{(P=0.99)}$ value corresponds to L_{max} , and Equation (9) is rewritten as

$$x_{(P=0.99)} = L_{max} = \delta y_{(0.99)} + \lambda \quad (14)$$

The δ and λ parameters are calculated using the maximum likelihood method ML from the log of the distribution function:

$$LL = \sum_{i=1}^n \ln \left(\frac{1}{\delta} \right) - \left(\frac{x_i - \lambda}{\delta} \right) - \exp \left(- \frac{x_i - \lambda}{\delta} \right) \quad (15)$$

The estimated parameters are referenced as λ_{ML} and δ_{ML} and are used to construct the best-fit line through the data points using Equation (9).

The standard error SE for any inclusion of length x is

$$SE_x = \delta_{ML} \sqrt{(1.109 + 0.514y + 0.608y^2) / n} \quad (16)$$

The approximate 95% confidence interval is given by

$$95\% \text{ CI} = \pm 2 SE(x) \quad (17)$$

The comparison of differences in sizes of large inclusions in two steels, denoted A and B , is calculated by the approximate 95% confidence interval for $L_{max}(A) - L_{max}(B)$ by the following equation:

$$C.I = L_{max}(A) - L_{max}(B) \pm 2\sqrt{S.E_{ref}(A)^2 + S.E_{ref}(B)^2} \quad (18)$$

If the lower to upper bounds of the 95% CI include 0, then it is concluded that there is no difference in the characteristic sizes of the largest inclusions in heats A and B .

3. Materials and Methods

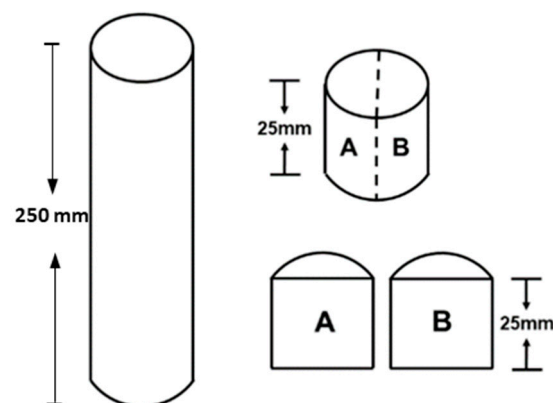
Measurements and analyses of inclusion size distributions in wire rod specimens from six plant-scale heats were conducted. The PDF approach was used to analyze the whole size distribution, and GEV theory was employed to analyze the upper tail of the size distributions.

Specimens from six different heats of high carbon rod wire produced at the plant scale were studied. The heats were produced by an electric arc furnace-ladle treatment-degassing-continuous casting route, and the liquid steel was deoxidized with Si. The studied steel corresponded to SAE 9254, and Table 1 shows the chemical composition expressed in weight percent (wt. %) for two specimens of each heat. The chemical analysis of C and S was performed using the infrared combustion technique, while the content of other elements was determined using the spark emission spectroscopy technique.

Table 1. Chemical composition (wt. %) of the studied heats.

Heat	Specimen	Content (wt. %)					
		C	Mn	Si	Cr	P	S
1	1	0.57	0.70	1.45	0.66	0.008	0.014
	2	0.58	0.70	1.44	0.67	0.007	0.012
2	1	0.54	0.68	1.43	0.65	0.008	0.014
	2	0.57	0.70	1.45	0.66	0.007	0.014
3	1	0.64	0.71	1.51	0.71	0.009	0.019
	2	0.65	0.72	1.52	0.71	0.009	0.019
4	1	0.59	0.70	1.5	0.70	0.008	0.019
	2	0.60	0.71	1.48	0.69	0.008	0.019
5	1	0.60	0.70	1.5	0.66	0.007	0.17
	2	0.58	0.71	1.52	0.70	0.008	0.17
6	1	0.54	0.71	1.52	0.71	0.009	0.15
	2	0.61	0.70	1.49	0.69	0.008	0.15

Inclusion size distributions were estimated using the metallographic procedure detailed in the ASTM E2283 standard, which was rigorously followed. For each heat, six specimens of wire rod in as-rolled conditions of 25 mm diameter and 200 mm length were available. Each specimen was cut into a probe of 25 mm length and sectioned longitudinally as shown in Figure 1. The plane denoted as A was progressively dry ground using 80-, 220-, 300-, 500-, 800-, 1000-, and 1200-grit SiC paper and polished with 3 and 1 μm diamond paste. The measurements were conducted under a Nikon Eclipse MA200 light optical microscope (Minato ku, Japan) at 100X magnification on 150 fields by image analysis, and the total analyzed surface was 150 mm². Three additional planes were analyzed, ensuring that the space between neighboring planes was at least 0.3 mm, thus avoiding inclusions being counted more than once. The total number of analyzed fields per heat was 600.

**Figure 1.** Obtention of probes for metallographic measurements.

The totality of the analyzed inclusions in each heat was considered to estimate the corresponding PDF using Equation (1). The frequency of inclusions per volume unit specified in that equation was estimated from the two-dimensional inclusion measurements obtained by image analysis, which were transformed into three-dimensional data using a procedure based on the Saltikov method [16,17].

By applying the ASTM E2283 standard, the measured maximum inclusion size in each of the inspected planes (24) was used for the statistical analyses described in the standard and synthesized in the previous section of this paper.

4. Results and Discussion

Figure 2 shows the measured inclusion frequency (inclusions/mm²) and area fraction for the six specimens of each heat. In general, Heats 5 and 6 presented the highest values for both parameters, whereas Heats 1 and 2 presented the lowest values. Furthermore, Heats 5 and 6 showed more variability among specimens of the values of both parameters.

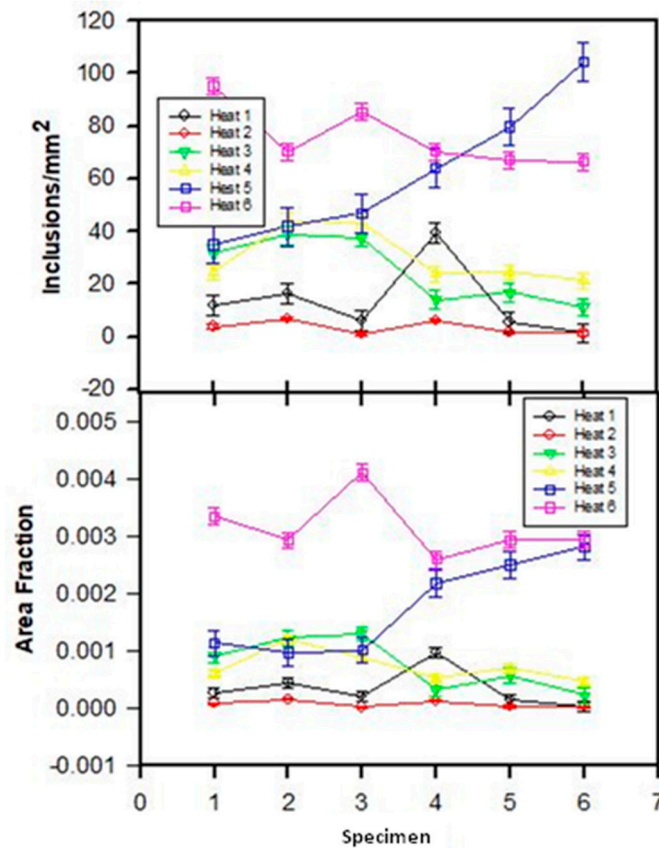


Figure 2. Evolution of inclusions/mm² and area fraction of inclusions.

4.1. Population Density Function PDF

Figure 3 shows the calculated PDF for each heat. The inclusion size is referred to as the inclusion equivalent diameter, which is defined as the diameter of a circle with the same area as the recorded particle [5]. Great differences were observed at small inclusion sizes, which decreased as the inclusion size increased. Below 10 μm , Heat 2 presented the lowest PDF values and was followed by Heats 1 and 3, while the rest of the heats presented similar values. In the range of 10–20 μm , Heat 2 continued to present the lowest values, followed by Heat 1, whereas Heat 6 presented the highest values; the rest of the heats presented similar values. Furthermore, the magnification of the PDF scale (inner figure) shows that at larger inclusion sizes, differences are also observed in PDF values and that Heats 2 and 6 showed the lowest and highest values of PDF, respectively. Thus, it can be stated for the studied heats that as the frequency of small inclusions increased, the population of large inclusions also increased, i.e., that the presence of large inclusions was due to the processing of liquid steel rather than to an eventual phenomenon.

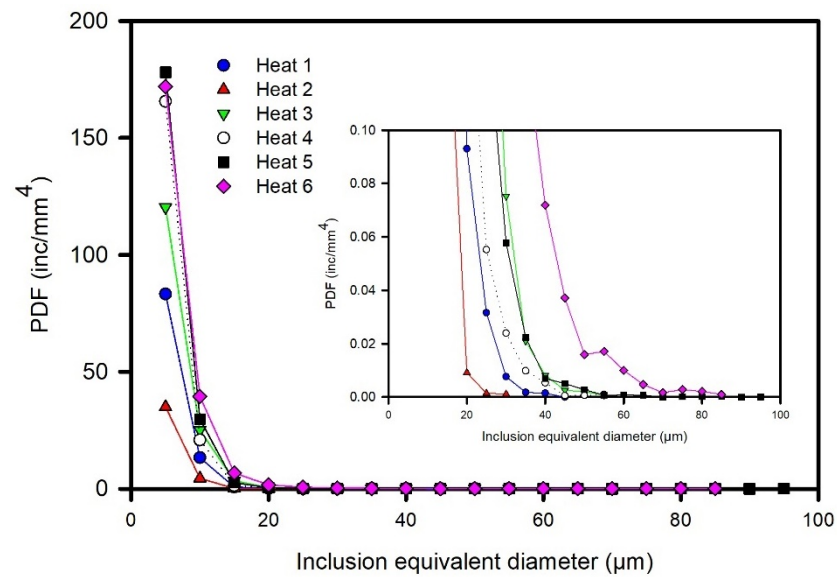


Figure 3. Evolution of the population density function PDF.

The logarithmic representation of the calculated PDFs is shown in Figure 4. A general linear power law behavior, represented by a reference straight line plotted in the figure, was observed. The reference straight line was estimated from the totality of the PDF data. The most notable deviations from the reference line corresponded to Heats 2 and 6, respectively, whereas the other heats fit better to the reference line. To clarify the observed behavior, the logarithmic representations of the PDFs of Heats 2 and 6 are shown in Figure 5, in which the data of Heat 4 were included because of its better fit to the reference line. Heat 6 presented both a higher frequency of inclusions and a larger inclusion size; in contrast, Heat 2 presented a lower frequency of inclusions and a smaller inclusion size, and Heat 4 exhibited intermediate values of both parameters. To individually analyze the heats of Figure 5, the data corresponding to the associated six samples of each heat are shown in Figure 6. As expected from a statistical point of view, more dispersion between the data were observed as the frequency decreased (Heat 2), although the linear trend continued to be observed. Thus, the heats can be ordered in decreasing order of cleanliness as follows: Heat 2, 4 and 6. Furthermore, Heats 3 and 5 had a similar behavior to Heat 4.

Then, the differences between the slopes of the straight lines of each heat can be deduced. The slope of the straight line is associated with the refining process and is specific to each process. Van Ende et al. [5] showed results for Ti-alloyed Al-killed steel produced in different plants. At the end of the refining process, a linear behavior of log PDF with a good fit was shown, and the slope values of the straight line were similar regardless of the plant of production. The slope value (-3.5) was associated with the Al-deoxidation process. Thus, the average slope value of the reference line (-0.089) in Figure 4 can be associated with the Mn–Si deoxidation process. In previous work [18], $\text{SiO}_2\text{-Al}_2\text{O}_3\text{-MnO}$ inclusions were observed at the beginning of the ladle treatment, which evolved to $\text{SiO}_2\text{-Al}_2\text{O}_3\text{-CaO-MgO}$ inclusions during treatment. Of note, $\text{SiO}_2\text{-Al}_2\text{O}_3\text{-CaO-MgO}$ inclusions were observed in this work under as-rolling conditions, as shown in Figure 7 for inclusions of different sizes. This result suggests that the estimated slope of the reference line is associated with the formation of $\text{SiO}_2\text{-Al}_2\text{O}_3\text{-MnO}$ inclusions during the Mn–Si deoxidation process and their evolution to $\text{SiO}_2\text{-Al}_2\text{O}_3\text{-CaO-MgO}$ inclusions during ladle treatment. Furthermore, the linear behavior indicates that the new inclusions were not formed after liquid steel treatment and that inclusion populations evolved by the growth of inclusions, breakage, and removal of inclusions. In addition, the inclusions found in all samples were embedded in a matrix similar to that presented in Figure 8. The microstructure of the matrix did not vary due to the similarity of the chemical composition (Table 1) and because the inclusions were subjected to the same thermomechanical treatment.

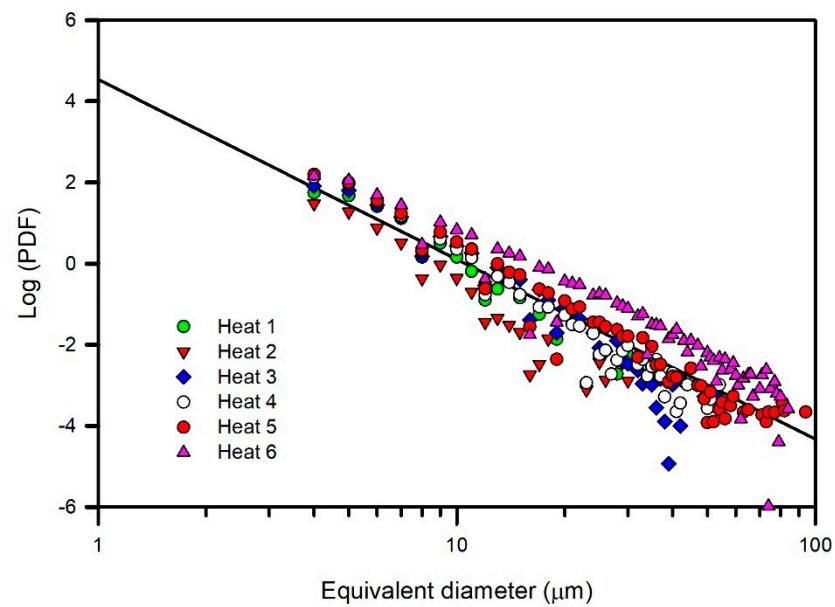


Figure 4. Log-log plots of PDFs versus inclusion equivalent diameter for all heats.

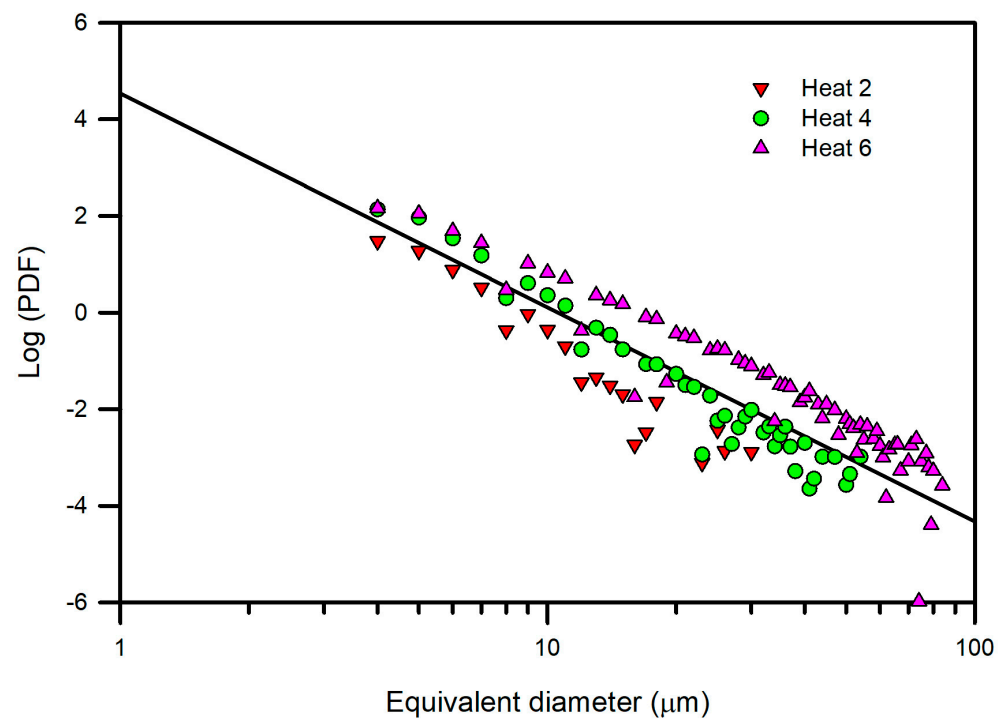


Figure 5. Log-log plot of PDFs versus inclusion equivalent diameter for Heats 2, 4 and 6.

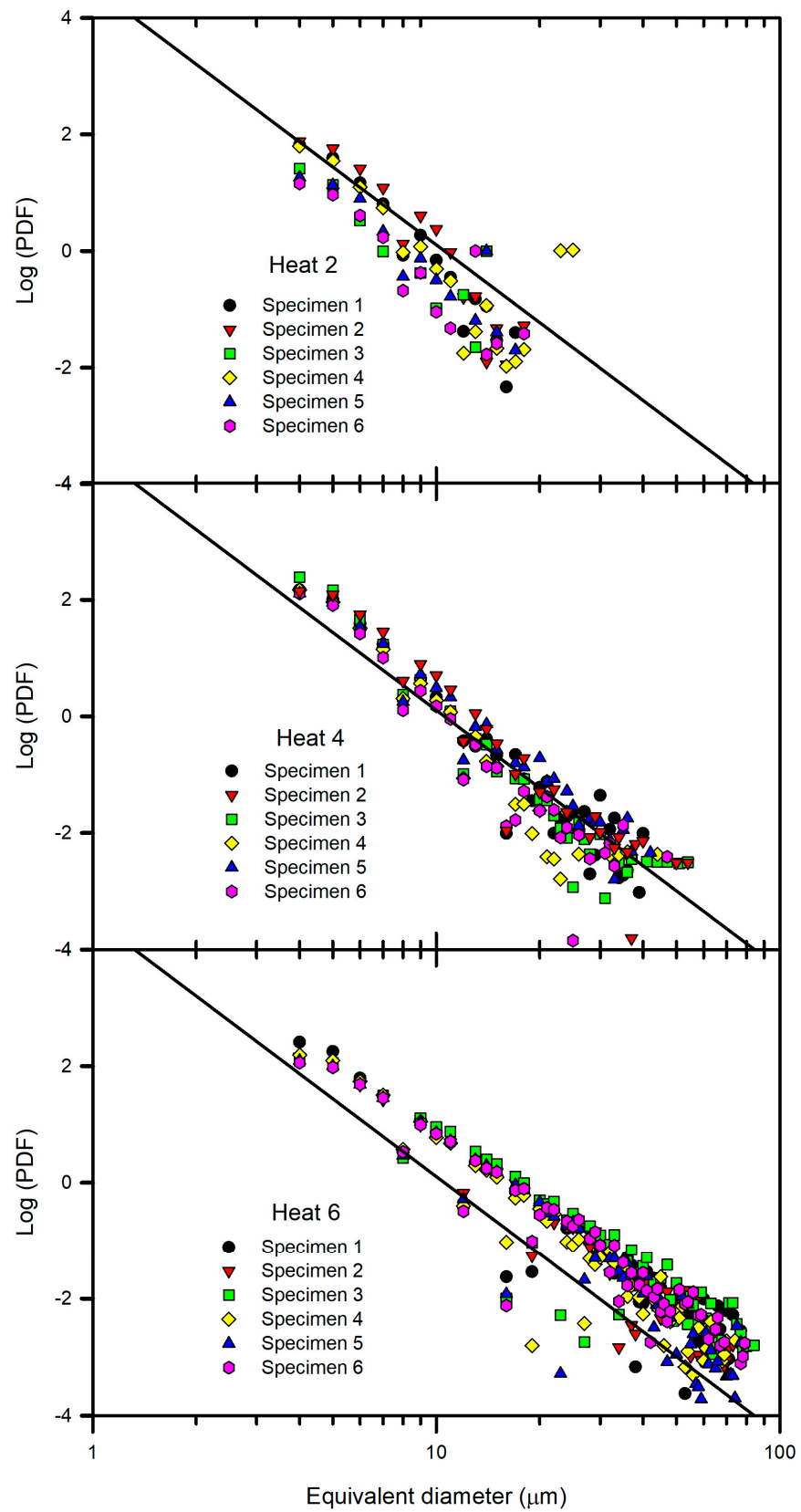


Figure 6. Log-log plot of PDFs versus inclusion equivalent diameter for specimens of Heats 2, 4 and 6.

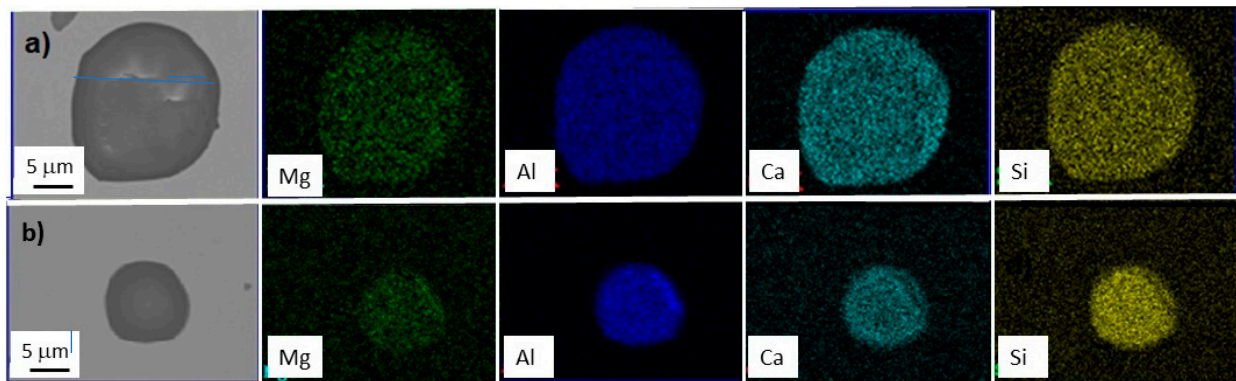


Figure 7. Elemental mapping for $\text{SiO}_2\text{-Al}_2\text{O}_3\text{-CaO-MgO}$ inclusions of different sizes: (a) 20 μm and (b) 12 μm .

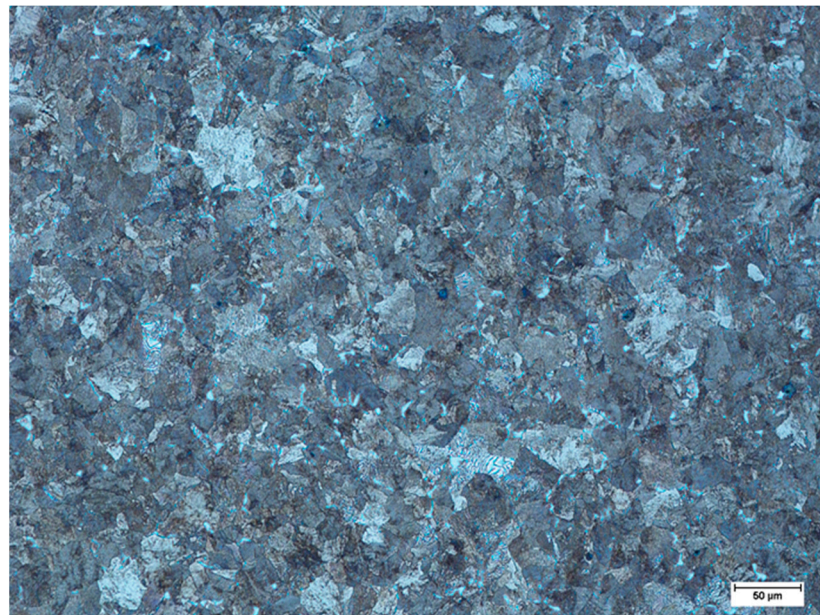


Figure 8. Typical microstructure of the steel matrix for the studied heats.

4.2. Extreme Value Distribution Analysis

Figure 9 shows a representation of the inclusion size distribution in histogram format. In this section, “length inclusion” is used to denote the inclusion size, just as the ASTM E2283 standard does. Of note, the inclusion length corresponds to the “equivalent diameter” used in the previous section. Two main observations can be highlighted. Below 20 μm , the highest frequency was shown by Heat 2; above 70 μm , however, Heat 6 had the highest frequency. For intermediate inclusion sizes, it is difficult to describe a trend.

Table 2 shows the 24 measured values of maximum inclusion length obtained for each heat from four analyzed planes in each of the six available specimens. The maximum inclusion length values are listed in increasing order as specified by the ASTM E2283 standard. The reduced variate was calculated using Equation (11) and is shown in Figure 10 for each heat as a function of the inclusion length. In general, a linear behavior for individual heats was observed. The fit of the straight lines was better at small inclusion lengths, and scattering was observed at longer inclusion lengths. It is also observed that steeper slopes correspond to lines located at shorter inclusion lengths, and consequently, the interception with the horizontal axis was different for each line.

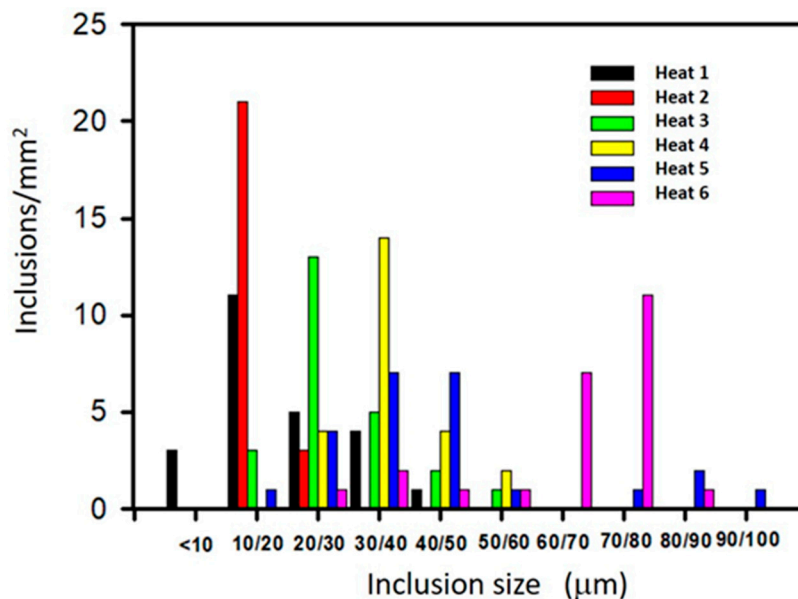


Figure 9. Inclusion size distribution.

Table 2. Inclusion maximum length L_{max} (µm) for analyzed plans in each heat.

N° Inclusion	Heat					
	1	2	3	4	5	6
1	7.5	10.4	16.7	20.2	16.7	24.8
2	8.1	11.0	19.0	20.8	21.4	36.9
3	8.7	11.5	19.6	24.8	25.4	39.2
4	10.4	11.5	20.2	26.0	26.0	43.9
5	11.6	12.1	20.2	31.2	26.5	57.1
6	12.1	12.7	20.8	31.7	31.2	60.6
7	12.1	12.7	20.8	31.7	31.7	64.0
8	12.1	13.3	21.4	32.9	34.0	64.0
9	12.7	13.3	22.5	32.9	34.6	64.6
10	14.4	13.3	23.1	32.9	35.2	65.8
11	15.0	14.4	23.7	33.45	35.2	69.8
12	15.0	14.4	24.2	34.0	39.2	69.8
13	17.3	14.4	24.8	34.6	40.4	71.0
14	19.0	15.0	25.4	35.2	45.0	72.1
15	21.9	16.2	30.0	35.8	46.2	73.3
16	22.5	16.2	30.0	35.8	46.7	75.0
17	23.7	16.2	31.7	39.8	47.9	75.0
18	26.5	17.9	32.3	39.8	48.5	76.2
19	30.0	17.9	34.0	41.5	49.0	77.9
20	31.7	17.9	35.2	43.3	50.8	77.9
21	32.9	17.9	38.1	46.2	73.0	78.5
22	38.1	22.6	42.7	49.0	80.2	79.0
23	38.7	24.2	48.5	53.1	80.8	79.6
24	40.4	29.4	52.5	53.7	93.5	83.1

Table 3 lists the values of the estimated statistical parameters according to the procedure of the ASTM E2283 standard. The values of λ , δ , and L_{max} are plotted in Figure 11, in which it is observed that the lower the values of λ and δ are, the lower are the values of L_{max} . Thus, the heats can be listed in increasing order of L_{max} values as follows: Heat 2, Heat 1, Heat 3, Heat 4, Heat 5, and Heat 6. This behavior is illustrated in Figure 12, where the probability distribution functions calculated via Equation (5) and using the values of λ and δ included in Table 3 are plotted.

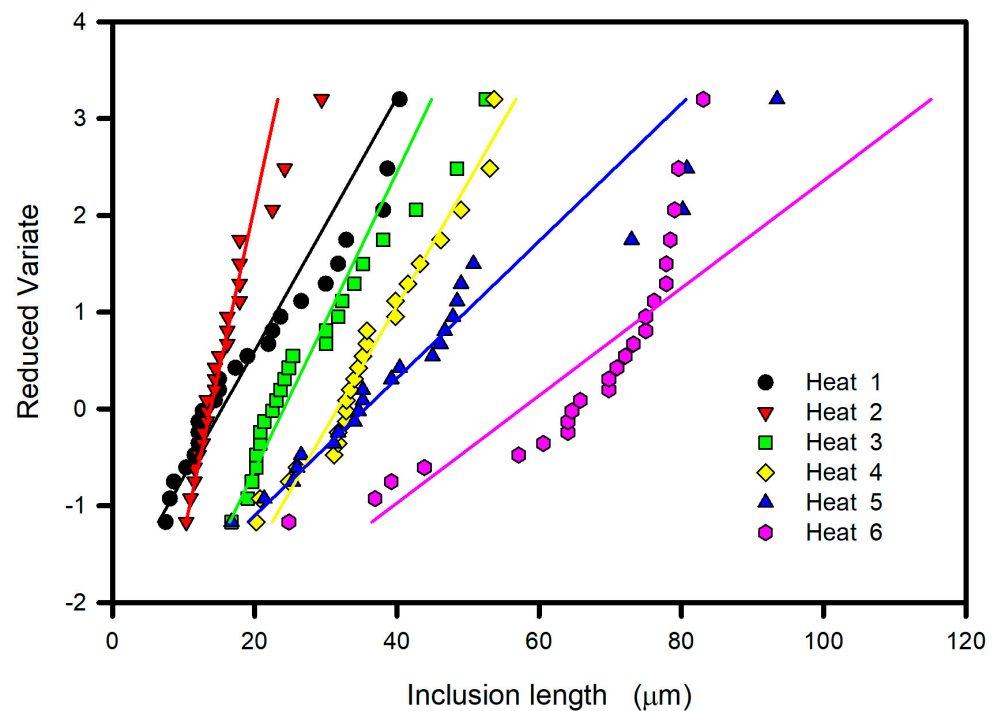


Figure 10. Reduced variate versus inclusion length.

Table 3. Values of statistical parameters (μm).

Parameters	Heat					
	1	2	3	4	5	6
λ	15.4	13.8	24.1	32.2	35.6	57.5
δ	7.6	2.9	6.5	8.8	14.1	18.0
<i>L</i> average	20.0	15.7	28.2	35.8	44.1	65.8
Standard deviation (Sdev)	10.4	4.6	9.6	11.8	19.8	15.3
Maximum length (L_{max})	68.2	34.2	69.0	92.7	132.9	181.9
Minimum length Y (L_{min})	6.9	6.9	6.9	6.9	6.9	6.9
Standard error (S.E.)	8.9	3.5	7.7	10.4	16.7	21.3

To determine whether the observed differences in L_{max} values were statistically significant, L_{max} values were compared according to the procedure described in the ASTM E2283 standard. The criterion of a 95% C.I. was calculated from the predicted value of L_{max} for each heat as well as the corresponding standard error. Table 4 lists the results of a round-robin comparison in matrix format, where the column and arrow titles correspond to the identification of heats. The interception of a column with an arrow denotes the range of bounds of the 95% C.I. of the corresponding heats. A C.I. range that does not include 0 is denoted in red and indicates a difference between the compared L_{max} ; otherwise, it is denoted in green and indicates that there was no difference. The L_{max} of Heats 5 and 6 did not differ from each other; in contrast, they differed from the L_{max} of the rest of the heats. Furthermore, L_{max} of Heat 2 was different from other L_{max} , and L_{max} of Heats 1, 3 and 4 were not different from each other. Thus, using the L_{max} parameter as the cleanliness index, it can be stated that Heat 2 is the cleanest and significantly different from the rest of the heats; Heats 5 and 6 are the worst and significantly different from the rest of the heats; Heats 1, 3 and 4 are not different from each other, and their inclusion cleanliness is intermediate between Heat 2 and Heats 5 and 6.

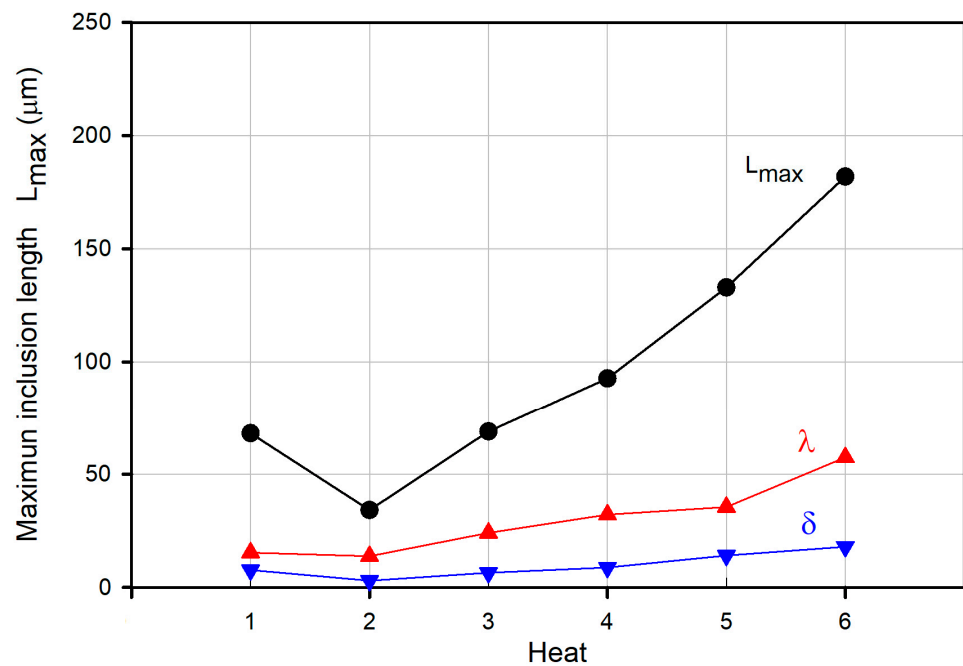


Figure 11. Maximum inclusion size L_{max} , λ , and δ for all heats.

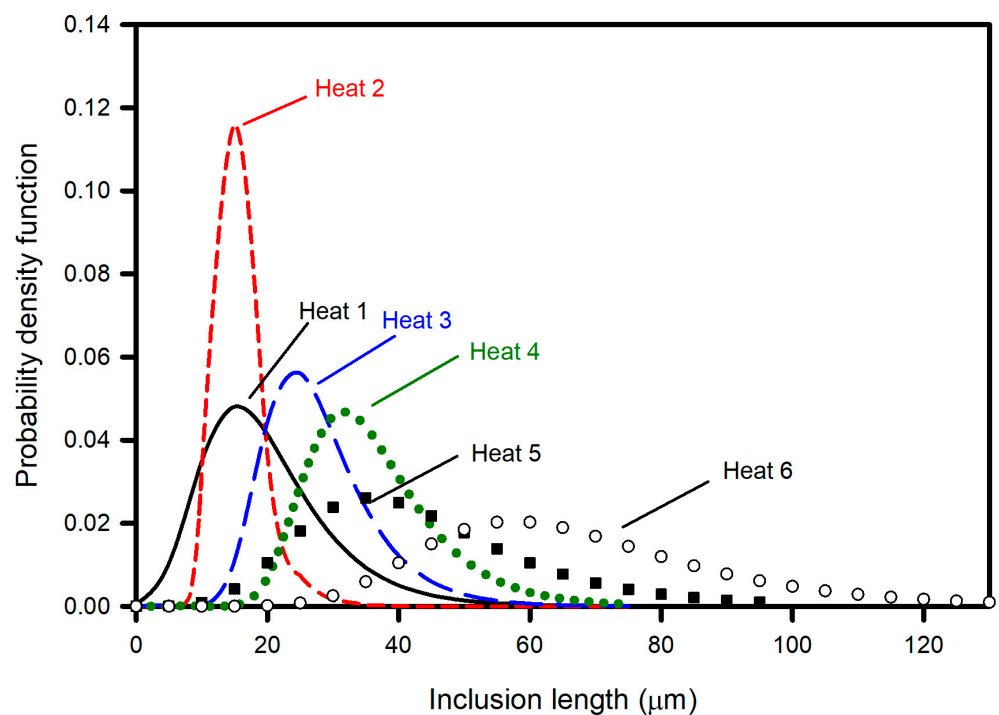


Figure 12. Probability density function for heats.

Although L_{max} represents a useful indicator that enables the comparison and discrimination of inclusion populations, there is often interest in knowing the probability of finding inclusions greater than a certain “critical” size depending on the specific application of the steel component. For example, in components subjected to fatigue, it is accepted that the size of the inclusion is important because cracks can form at the inclusion–steel interface. In this context, the survival function $S_{(x)}$ (probability of finding an inclusion larger than a given length, equal to the complement of the cumulative density function) rather than L_{max} is more convenient. Figure 13 presents $S_{(x)}$ as a function of the inclusion length for all heats. The order of heats previously stated as a function of L_{max} is confirmed for inclusion

lengths greater than 35 μm , where no overlapping of curves is observed. At 35- and 10 μm inclusion lengths, the curves of Heats 3 and 4 and Heats 1 and 2 overlapped, and therefore, the order of heats was modified.

Table 4. Range of bounds of 95% confidence interval C.I.

	Heat 2	Heat 3	Heat 4	Heat 5	Heat 6
Heat 1	53.23	22.82	2.87	−26.84	−67.43
	14.79	−24.40	−51.96	−102.63	−159.96
Heat 2		−17.89	−36.64	−64.63	−104.49
		−51.70	−80.46	−132.87	−190.94
Heat 3			2.10	−27.18	−67.56
			−49.60	−100.72	−158.26
Heat 4				−0.87	−41.71
				−79.52	−136.60
Heat 5					5.21
					−103.14

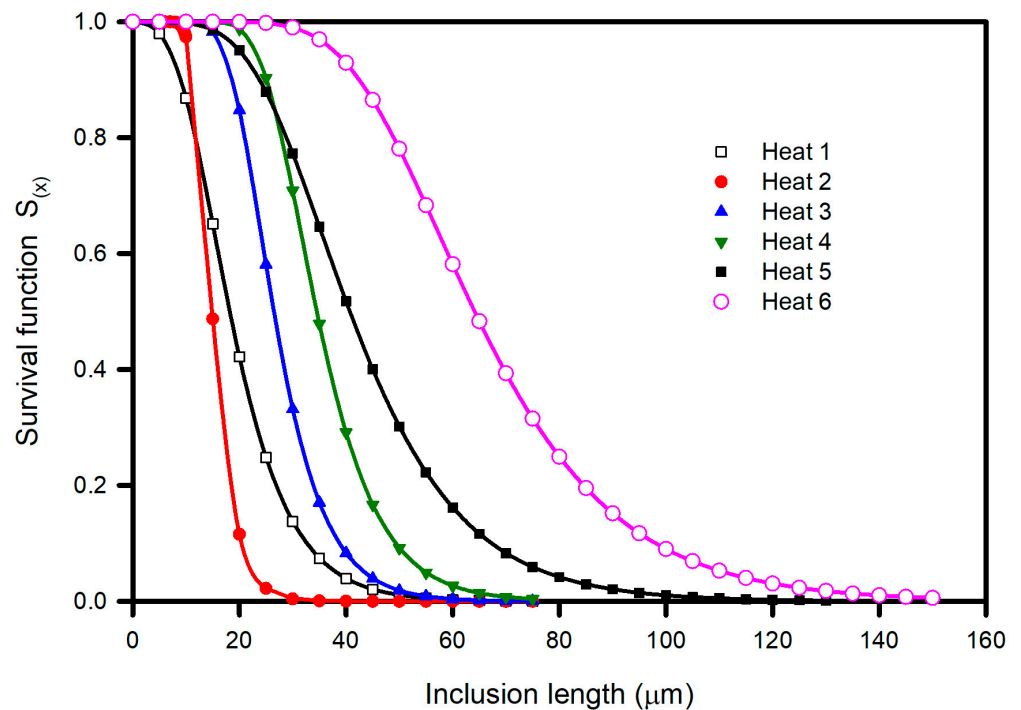


Figure 13. Survival function $S_{(x)}$ for each heat.

$S_{(x)}$ is plotted in Figure 14 from the data of Figure 13 for three critical inclusion lengths: 10, 20 and 30 μm . The heats can be ordered by increasing the $S_{(x)}$ value for each critical value; for example, for an inclusion length shorter than 10 μm , the order is Heat 1, Heat 2, Heat 3, Heat 4, Heat 5 and Heat 6. This order is altered when the critical value of 20 μm is selected, changing the order to Heat 2, Heat 1, Heat 3, Heat 5, Heat 4 and Heat 6. The observed difference is explained by the overlapping probability density curves and $S_{(x)}$ curves for Heats 1 and 2 and for Heats 4 and 5. For example, in Heat 1 and Heat 2, overlapping can be observed in the upper left corner in Figure 13, or the overlapping of probability density functions in the lower left corner in Figure 11. The same explanation can be used for the inversion of order between Heats 4 and 5. Furthermore, for critical values greater than 35 μm , where no overlapping of curves is observed, the order is Heat 2, Heat 1, Heat 3, Heat 4, Heat 5 and Heat 6. This is the same when parameter L_{max} is considered as the cleanliness parameter.

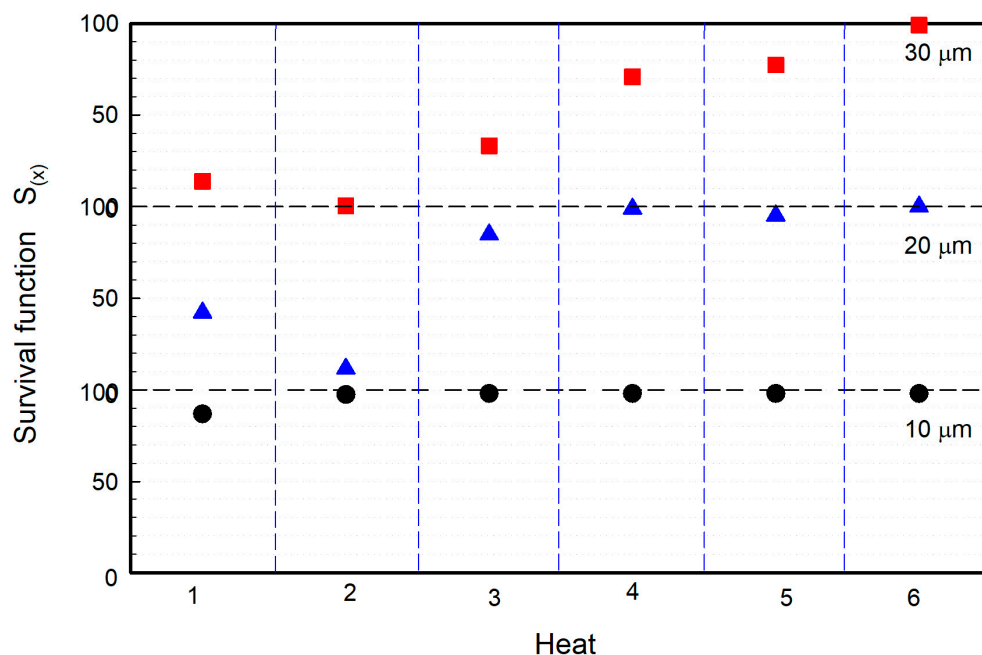


Figure 14. Survival function $S_{(x)}$ for different “critical” inclusion sizes.

5. Conclusions

Inclusion size distributions in wire rod specimens from six plant-scale heats were measured and analyzed. The measurements were taken following the metallographic procedure specified in the ASTM E2283 standard. The analysis of size distributions was developed using two approaches: (1) the estimation of PDFs according to the Higgins formalism [3] to obtain information on the whole inclusion size distribution and (2) the use of the extreme value theory to describe the upper tail of the size distributions. Thus, the following conclusions can be drawn.

- Heats were listed in decreasing order of inclusion cleanliness based on the analysis of the linear logarithmic representation of PDFs.
- No new inclusions were formed after the ladle treatment process, as inferred from the linear behavior of the logarithmic representation of PDFs, a power-law-type with time. Hence, the evolution of inclusion distribution was associated with growth, breakage, and the removal of inclusions.
- Heats were listed in decreasing order of inclusion cleanliness using the maximum inclusion length parameter L_{max} . The use of the extreme value statistics procedure specified in the ASTM E2283 standard led to a statistical comparison of L_{max} .
- Heats were ordered by considering the survival function $S_{(x)}$ values (probability of finding an inclusion larger than a “critical” inclusion length) estimated using the GEV theory. It was shown that the order can change depending on the critical value.

Author Contributions: P.H.-E. performed the experimental measurements and calculations and prepared the first draft; M.H.-T. analyzed the data and wrote the final manuscript; M.d.J.C.-R. participated in the image analysis and data analysis in the context of CONACyT Grant A1-S-44269; J.R.-M. participated in the data analysis and review of the manuscript. All authors have read and agreed to the published version of the manuscript.

Funding: P. Huazano-Estrada acknowledges the Ph.D. scholarship provided by the National Council of Science and Technology of Mexico (CONACyT) for the realization of this work.

Acknowledgments: M. Herrera-Trejo acknowledges Ternium for providing the facilities for this work.

Conflicts of Interest: The authors declare no conflict of interest.

References

1. Kaushik, P.; Lehmann, J.; Nadif, M. State of the Art in Control of Inclusions, Their Characterization, and Future Requirements. *Met. Mater. Trans. A* **2012**, *43*, 710–725. [[CrossRef](#)]
2. Pretorius, E.B.; Oltmann, H.G.; Scharf, B.T. An Overview of Steel Cleanliness from an Industry Perspective. In *AISTech Proceedings 2013*; Association for Iron and Steel Technology: Warrendale, PA, USA, 2013; pp. 6–9.
3. Higgins, M. Measurement of crystal size distributions. *Am. Miner.* **2000**, *85*, 1105–1116. [[CrossRef](#)]
4. Atkinson, H.V.; Shi, G. Characterization of Inclusions in Clean Steels: A Review Including the Statistics of Extremes Methods. *Prog. Mater. Sci.* **2003**, *48*, 457–520. [[CrossRef](#)]
5. Van Ende, M.-A.; Guo, M.; Zinngrebe, E.; Blanpain, B.; Jung, I.-H. Evolution of Non-Metallic Inclusions in Secondary Steelmaking: Learning from Inclusion Size Distributions. *ISIJ Int.* **2013**, *53*, 1974–1982. [[CrossRef](#)]
6. Zinngrebe, E.; Van Hoek, C.; Visser, H.; Westendorp, A.; Jung, I.H. Inclusion Population Evolution in Ti-alloyed Al-killed Steel during Secondary Steelmaking Process. *ISIJ Int.* **2012**, *52*, 52–61. [[CrossRef](#)]
7. Bindeman, I.N. Fragmentation Phenomena in Populations of Magmatic Crystals. *Am. Miner.* **2005**, *90*, 1801–1815. [[CrossRef](#)]
8. Piva, S.; Pistorius, P. Ferrosilicon-Based Calcium Treatment of Aluminum-Killed and Silicomanganese-Killed Steels. *Metall. Mater. Trans. B* **2021**, *52*, 6–14. [[CrossRef](#)]
9. Shu, Q.; Alatarvas, T.; Visuri, V.-V.; Fabritus, T. Modelling the Nucleation, Growth and Agglomeration of Alumina Inclusion in Molten Steel by Combining Kampmann-Wagner Numerical Model with Particle Size Grouping Method. *Metall. Mater. Trans. B* **2021**, *52*, 1818–1829. [[CrossRef](#)]
10. Murakami, Y. Inclusion Rating by Statistics of Extreme Values and Its Application to Fatigue Strength Prediction and Quality Control of Materials. *Int. J. Fatigue* **1996**, *3*, 215. [[CrossRef](#)]
11. *ASTM E2283-08*; Extreme Value Analysis of Nonmetallic Inclusions in Steel and Other Microstructural Features. ASTM International: West Conshohocken, PA, USA, 2014.
12. Kumar, P.V.; Balachandran, G. Microinclusion Evaluation Using Various Standards. *Trans. Indian Inst. Met.* **2019**, *72*, 877–888. [[CrossRef](#)]
13. Fuchs, D.; Tobie TStahl, K. Challenges in Determination of Microscopic Degree of Cleanliness in Ultra-Clean Gear Steels. *J. Iron Steel Res. Int.* **2022**, *29*, 1583–1600. [[CrossRef](#)]
14. Meng, Y.; Li, J.; Wang, K.; Zhu, H. Effect of the Bloom-Heating Process on the Inclusion Size of Si-Killed Spring Steel Wire Rod. *Metall. Mater. Trans. B* **2022**, *53*, 2647–2656. [[CrossRef](#)]
15. Tian, L.; Liu, L.; Ma, B.; Zaïri, F.; Ding, N.; Guo, W.; Xu, N.; Xu, H.; Zhang, M. Evaluation of Maximum Non-Metallic Inclusion Sizes in steel by Statistics of Extreme Values Method Based on Micro-CT Imaging. *Metall. Res. Technol.* **2022**, *119*, 202. [[CrossRef](#)]
16. Gulbin, Y. On Estimation and Hypothesis Testing of the Grain Size Distribution by the Saltykov Method. *Image Anal. Stereol.* **2008**, *27*, 163–174. [[CrossRef](#)]
17. Takahashi, J.; Suito, H. Evaluation of the Accuracy of the Three-Dimensional Size Distribution Estimated from the Schwartz-Saltykov Method. *Metall. Mater. Trans. A* **2003**, *34*, 171–181. [[CrossRef](#)]
18. García-Carbajal, A.; Herrera-Trejo, M.; Castro-Cedeño, E.; Castro-Román, M.; Martínez-Enríquez, A. Characterization of Inclusion Populations in Mn-Si Deoxidized Steel. *Metall. Mater. Trans. B* **2017**, *48*, 3364–3373. [[CrossRef](#)]